AGU PUBLICATIONS

Geophysical Research Letters

RESEARCH LETTER
10.1002/2015GL064693

Special Section:
First Results from the MAVEN Mission to Mars

MAVEN observations of solar wind hydrogen deposition in the atmosphere of Mars

J. S. Halekas[1], R. J. Lillis[2], D. L. Mitchell[2], T. E. Cravens[3], C. Mazelle[4], J. E. P. Connerney[5], J. R. Espley[5], P. R. Mahaffy[5], M. Benna[5,6], B. M. Jakosky[7], J. G. Luhmann[2], J. P. McFadden[2], D. E. Larson[2], Y. Harada[2], and S. Ruhunusiri[1]

[1]Department of Physics and Astronomy, University of Iowa, Iowa City, Iowa, USA, [2]Space Sciences Laboratory, University of California, Berkeley, California, USA, [3]Department of Physics and Astronomy, University of Kansas, Lawrence, Kansas, USA, [4]L'Institut de Recherche en Astrophysique et Planétologie, Toulouse, France, [5]NASA Goddard Space Flight Center, Greenbelt, Maryland, USA, [6]CSST, University of Maryland, Baltimore County, Baltimore, Maryland, USA, [7]Laboratory for Atmospheric and Space Physics, University of Colorado Boulder, Boulder, Colorado, USA

Abstract Mars Atmosphere and Volatile EvolutioN mission (MAVEN) observes a tenuous but ubiquitous flux of protons with the same energy as the solar wind in the Martian atmosphere. During high flux intervals, we observe a corresponding negative hydrogen population. The correlation between penetrating and solar wind fluxes, the constant energy, and the lack of a corresponding charged population at intermediate altitudes implicate products of hydrogen energetic neutral atoms from charge exchange between the upstream solar wind and the exosphere. These atoms, previously observed in neutral form, penetrate the magnetosphere unaffected by electromagnetic fields (retaining the solar wind velocity), and some fraction reconvert to charged form through collisions with the atmosphere. MAVEN characterizes the energy and angular distributions of both penetrating and backscattered particles, potentially providing information about the solar wind, the hydrogen corona, and collisional interactions in the atmosphere. The accretion of solar wind hydrogen may provide an important source term to the Martian atmosphere over the planet's history.

Key Points:
- We observe H^+ and H^- in the atmosphere of Mars, at the solar wind energy
- Solar wind protons charge exchange and penetrate as ENAs then reconvert
- MAVEN can monitor hydrogen deposition and backscatter in the atmosphere

Correspondence to:
J. S. Halekas,
jasper-halekas@uiowa.edu

Citation:
Halekas, J. S., et al. (2015), MAVEN observations of solar wind hydrogen deposition in the atmosphere of Mars, *Geophys. Res. Lett.*, *42*, doi:10.1002/2015GL064693.

Received 24 MAY 2015
Accepted 15 JUN 2015

1. Introduction and Context

Mars, in addition to a collisional atmosphere at low altitude, has an exosphere (or "corona"), primarily composed of atomic and molecular hydrogen, which extends to many Martian radii [*Anderson*, 1974; *Chaufray et al*., 2008]. Given the relatively small Martian magnetosphere, extending only a few thousand kilometers from the planet's surface, a significant column of hydrogen extends upstream from the bow shock, exposed to the solar wind. As a result, charge exchange between incoming solar wind protons and planetary hydrogen forms a collimated beam of energetic neutral atoms (ENAs) with the original solar wind velocity, with fluxes (and densities) on the order of 1–3% of the solar wind [*Barabash et al*., 1995; *Kallio et al*., 1997; *Holmström et al*., 2002]. Fluxes of these ENAs will vary with solar wind flux; with solar cycle, seasonal, and short time scale changes in the exosphere [*Chaffin et al*., 2014]; and with solar wind-driven changes in the location of the bow shock that expose more or less of the corona to the solar wind.

Unlike the still-charged fraction of the solar wind, which is shocked, heated, and mostly deflected around the induced magnetosphere of Mars, the newly created ENAs do not respond to electromagnetic fields and can penetrate deep into the atmosphere. There, they undergo collisional interactions with atmospheric gases, eventually resulting in angular spreading, energy deposition, and backscattering of a portion of the distribution [*Kallio and Barabash*, 2001; *Kallio et al*., 2006; *Holmström et al*., 2002]. Mars Express (MEX) has comprehensively observed these hydrogen ENAs in the Martian system, including those produced in the solar wind and sheath [*Gunell et al*., 2006], the backscatter population [*Futaana et al*., 2006; *Mura et al*., 2007; *Wang et al*., 2013, 2014], and ENAs scattered into the planetary shadow [*Brinkfeldt et al*., 2006].

Inevitably, some fraction of both incoming and backscattered ENAs will interact with the atmosphere in charge-changing reactions, as discussed by *Kallio and Barabash* [2001]. Given MEX periapsis altitudes of ~270 km, well above the altitudes of peak energy deposition, most previous observations of protons inside the Martian magnetosphere probably represent direct penetration of hot ions from the magnetosheath, as

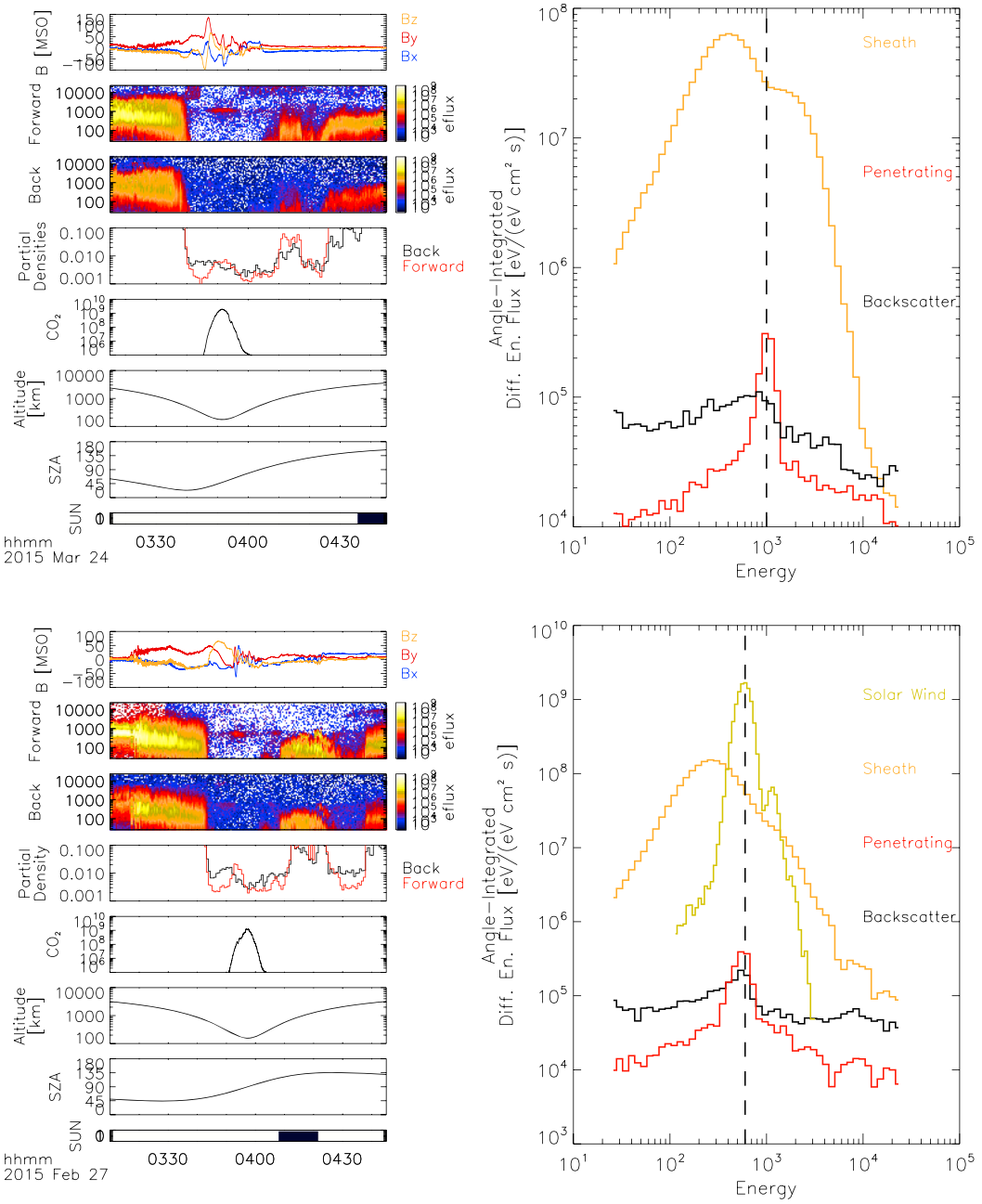

Figure 1. The time series plots show magnetic field components (nT), average ion differential energy flux (eV/(eV cm^2 s sr)) within 45° of antisunward (forward/penetrating flux), average ion differential energy flux in all other directions (backscatter), background-subtracted partial ion densities (cm^{-3}) computed for these two angular ranges for energies between 200 and 4000 eV, neutral CO_2 abundance (cm^{-3}), and spacecraft altitude and solar zenith angle for two orbit segments surrounding periapses on (top left) 24 March 2015 and (bottom left) 27 February 2015. (top right) Angle-integrated ion spectra for the sheath (03:30–03:35) and penetrating and backscatter populations near periapsis (03:44–03:57) for the 24 March orbit. (bottom right) Angle-integrated ion spectra from the solar wind (03:15–03:16:30), the sheath (03:25–03:30), and penetrating and backscatter populations near periapsis (03:50–04:00) for the 27 February orbit.

concluded by *Diéval et al.* [2012, 2013], but MEX may also have observed some reconverted protons. Mars Atmosphere and Volatile EvolutioN mission (MAVEN)'s lower altitude orbit now provides us with an opportunity to measure the products of penetrating hydrogen ENAs deep in the Martian atmosphere, including both positive and negative charge states. The energy and flux of these particles enable remote monitoring of the upstream solar wind, and their angular and energy spectra provide diagnostic

information on collisional processes in the atmosphere. In addition, by extrapolating from the charged fraction to the total ENA abundance, we can infer the solar wind hydrogen deposition in the Martian atmosphere as a function of time.

2. Penetrating Solar Wind Hydrogen Observed by MAVEN

On virtually every orbit through the dayside atmosphere below altitudes of a few hundred kilometers, MAVEN observes a tenuous population of positively charged ions with the same velocity as the upstream solar wind. Composition measurements (not shown) from the STATIC instrument [*McFadden et al*., 2015] indicate that these ions are protons, consistent with the reconverted solar wind hydrogen ENAs described above. Figure 1 shows observations from two representative orbits by the Solar Wind Ion Analyzer instrument [*Halekas et al*., 2013], with supporting information from the magnetometer instrument [*Connerney et al*., 2015]. The first orbit (Figure 1, top), with periapsis at low solar zenith angle in a region with moderate crustal magnetic fields, shows a nearly monoenergetic peak at 1 keV in the antisunward energy spectra (ions traveling in the original solar wind direction), centered at periapsis, and extending to a few hundred kilometers in altitude. In addition to the narrow peak at the solar wind energy, the penetrating spectra display a broad halo of lower fluxes extending to higher and lower energies, possibly produced by ENAs from charge exchange with the heated magnetosheath population [*Gunell et al*., 2006]. Though difficult to see in the time series, aggregate spectra integrated over the periapsis orbit segment also reveal an accompanying backscatter population with a degraded spectral form consistent with previous modeling [*Kallio and Barabash*, 2001], implying numerous collisional interactions in the atmosphere, and a significant hydrogen albedo (i.e., reflection of incoming hydrogen). Densities of the penetrating particles increase significantly near periapsis, implying that these particles could not have traveled though the intermediate altitude range in charged form. We observe the highest penetrating proton density at periapsis (~160 km), also the location of the highest neutral CO_2 density measured by Neutral Gas and Ion Mass Spectrometer (NGIMS) [*Mahaffy et al*., 2014], and thus consistent with electron stripping of incoming ENAs in the atmosphere. However, the density of penetrating protons does not increase as quickly with decreasing altitude as neutral density, indicating that back reactions (charge exchange) also play a role. We do not sample the undisturbed solar wind during this orbit, but the observed sheath spectra appears consistent with a solar wind energy the same as the penetrating population.

The second orbit (Figure 1, bottom) has a different geometry, with periapsis near the terminator, in a region of very weak crustal magnetic fields. In this case, the column of atmosphere with which the ENAs have interacted increases, and we observe a two-peaked pattern of penetrating protons with a first maximum well sunward of periapsis and a minimum at periapsis. This implies significant absorption and/or backscatter of the penetrating population, consistent with the high backscattered flux observed sunward of the first peak in penetrating flux. A second peak in the penetrating proton flux, located after periapsis and just outside of the shadow boundary, likely represents the result of atmospheric occultation of the hydrogen ENAs, as discussed by *Kallio et al*. [2006]. Throughout the periapsis segment, we observe a scattered population with energies below that of the solar wind, probably representing a combination of backscattered protons from the atmosphere, and more diffuse charge exchange from sheath protons interacting with planetary hydrogen [*Gunell et al*., 2006]. This orbital geometry allows direct sampling of the solar wind just outside the bow shock, and the one-to-one energy correspondence provides strong evidence of a genetic relationship between the upstream solar wind and the penetrating population.

3. Spatial Distribution and Solar Wind Control of Hydrogen Deposition

The close correlation between the energy of the upstream solar wind and that of the penetrating protons persists throughout the MAVEN mission, as shown in Figure 2. Though not every MAVEN orbit samples both the dayside region below a few hundred kilometers and the upstream region outside of the bow shock, significant periods with coverage of both regions allow us to demonstrate a high degree of correlation. Indeed, a large fraction of the penetrating populations observed for altitudes of 150–250 km with energies between 200 and 4000 eV have an inferred flow speed within 15% of the upstream solar wind, when observed on the same orbit (red points in Figure 2). The few exceptions have speeds greater than that of the solar wind, corresponding to the penetration of energetic pickup ions. Not only do the

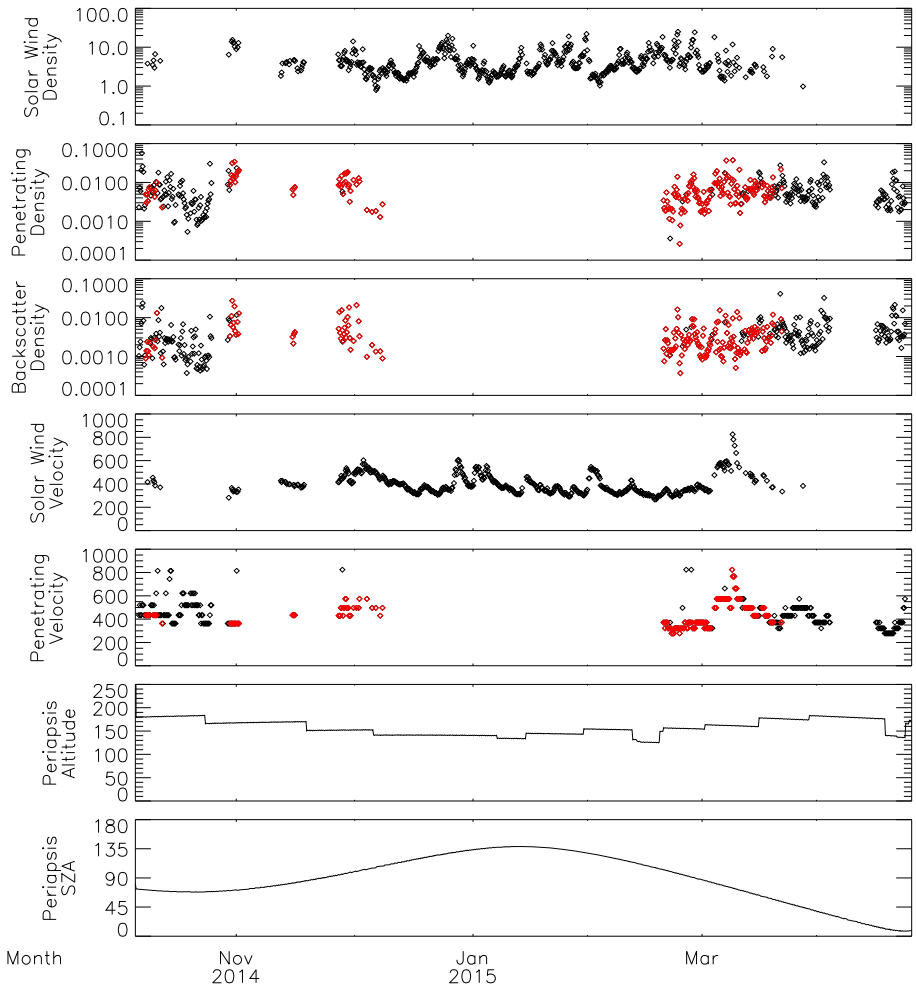

Figure 2. Upstream solar wind proton density, background-subtracted penetrating and backscatter proton density (cm^{-3}), upstream solar wind velocity (km/s), penetrating proton velocity (km/s), and periapsis altitude and solar zenith angle. Solar wind and penetrating/backscatter quantities represent orbit averages over undisturbed upstream intervals (when sampled by the MAVEN orbit) and sunlit portions of the orbit for altitudes 140–250 km (when sampled), respectively. Red points indicate values for which penetrating proton speeds match solar wind speeds (where available) to better than 15%.

speeds match extremely well but also the densities of both penetrating and backscatter populations at periapsis clearly track variations in the upstream solar wind density.

Though variations in density match qualitatively, the fraction of the upstream solar wind present in charged form in the lower atmosphere varies with solar wind flow energy, as shown in Figure 3. The ratio of the average penetrating proton density observed for altitudes of 150–250 km to the upstream solar wind density varies from 10^{-4} at low energies to values approaching 1% at higher energies. In contrast, the ratio between reflected and incident densities decreases with energy, consistent with the larger number of collisional interactions needed to alter the velocity of the incoming population. The observed ratio appears roughly consistent with the predicted hydrogen ENA albedo of 0.58 predicted by *Kallio and Barabash* [2001], though a quantitative comparison would have to take into account the energy loss of the observed backscatter population to determine an albedo. Note that the albedo should not exceed unity globally but can do so locally, especially near the terminator, where most backscatter flux comes from regions radially inward from the spacecraft but penetrating flux comes from the side at a glancing angle.

The total amount of solar wind hydrogen at periapsis (penetrating + backscatter), though not varying as steeply as the downgoing fraction, still varies by more than an order of magnitude. We can explain a large portion of this variability in terms of the energy dependence of electron stripping and charge exchange

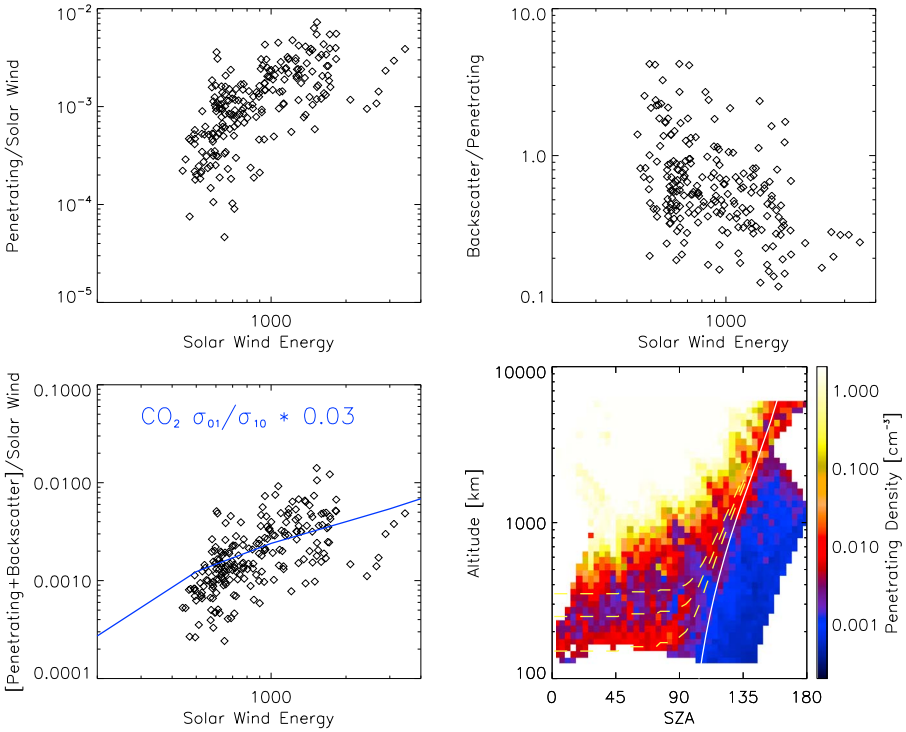

Figure 3. Ratios of (top left) penetrating proton to solar wind density, (top right) backscatter to penetrating density, and (bottom left) penetrating plus backscatter to solar wind density, all as a function of solar wind flow energy, for the orbit-averaged data points shown in red in Figure 2. The blue line shows the ratio between electron stripping and charge exchange cross sections for hydrogen in CO_2, multiplied by 0.03. (bottom right) Median background-subtracted penetrating proton partial densities computed from fluxes within 45° of antisunward and energies between 200 and 4000 eV, from 6 October 2014 to 22 April 2015. The solid white line indicates the light/shadow boundary at spacecraft altitude. The three dashed lines indicate contours of constant column density between the spacecraft and the Sun, assuming a spherically symmetric Martian neutral atmosphere with a scale height of 10 km.

cross sections for hydrogen in a dominantly CO_2 atmosphere [*Kallio and Barabash*, 2001]. If forward and backward reactions have reached equilibrium (but before significant energy loss has occurred), the ratio of these cross sections should correspond to the ratio between positively charged and neutral populations of hydrogen. Multiplying this ratio by the charge exchange efficiency of the solar wind with planetary hydrogen upstream from the bow shock should then provide the ratio between penetrating and solar wind proton flux. Figure 3 shows that the ratio of stripping to charge exchange from laboratory measurements [*Van Zyl et al.*, 1978; *Lindsay et al.*, 2005; *Kallio and Barabash*, 2001], multiplied by a nominal 3% upstream charge exchange efficiency appropriate for solar minimum [*Kallio et al.*, 1997], matches the observed trend. However, the data show a somewhat steeper drop in penetrating fluxes at low energy than this simple model. This decrease is opposite the expected trend for the upstream H^+-on-H charge exchange efficiency (which should increase slightly with decreasing energy [*Kallio et al.*, 1997]) and instead may result from changes in the hydrogen corona or magnetospheric structure. A change in the location of the bow shock provides a likely culprit; if the bow shock moves outward for low solar wind energies, less of the corona lies exposed to solar wind charge exchange, reducing the flux of ENAs and thus of reconverted protons at periapsis. Such a change in bow shock location could result from the dependence on solar wind dynamic pressure and/or Mach number [*Verigin*, 1999; *Edberg et al.*, 2009, 2010].

The spatial distribution of penetrating proton density further bolsters the case for an ENA source for the MAVEN observations. As shown in Figure 3, a superposed distribution of all observed 200–4000 eV antisunward partial densities displays a clear minimum at altitudes of ~250–400 km and a maximum at altitudes of 160–170 km, consistent with electron stripping of penetrating ENAs in the atmosphere (note that the diagonal "stripes" in this figure result from temporal variability in the input solar wind). If correct,

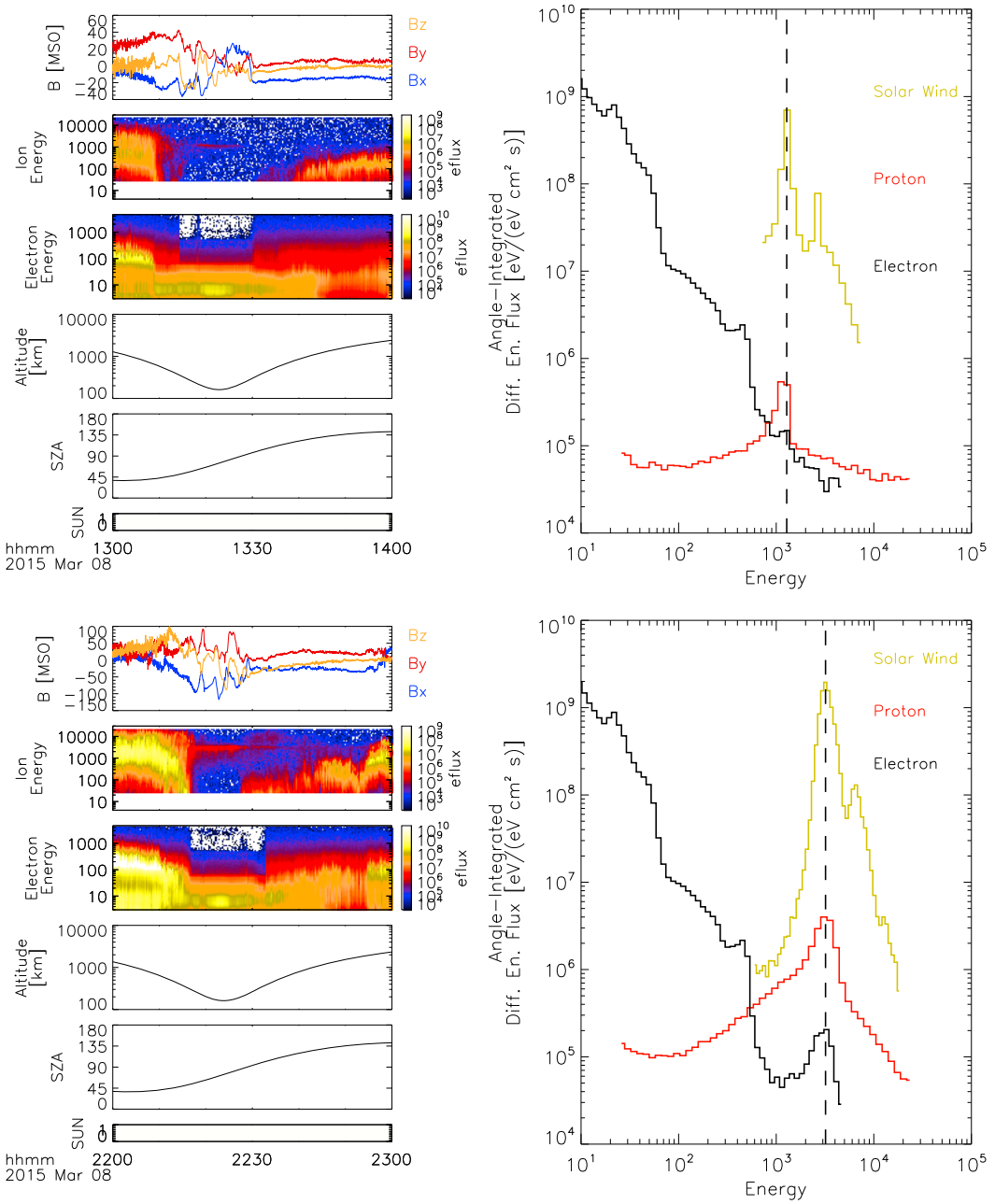

Figure 4. The time series plots show magnetic field (nT), ion and electron differential energy flux (eV/(eV cm^2 s sr)), and altitude and solar zenith angle, for two periapses on 8 March 2015, before/after the passage of a coronal mass ejection. (top right) Angle-integrated spectra for the solar wind (12:26–12:30) and ions and electrons near periapsis (13:20–13:30) for the pre-CME orbit. (bottom right) Angle-integrated spectra from the solar wind (21:32–21:34) and ions and electrons near periapsis (22:18–22:27) for the post-CME orbit.

densities of penetrating particles should scale with the total column of atmosphere encountered by incoming ENAs. Indeed, the data appear at least qualitatively consistent with this expectation, with penetrating densities roughly organized by isocontours of constant column density (which have a nearly constant altitude for solar zenith angles below 75°, but rise steeply in altitude past the terminator, due to occultation of ENAs through the limb atmosphere). This suggests that one should observe reconverted protons not only at periapsis but also just outside of the shadow boundary at high altitudes in the tail, as in the second orbit of Figure 1 (though plasma sheet ions can also exist in this region, partially obscuring

the narrow "trough" between sheath and penetrating populations). Smaller densities inside the shadow boundary may result from ENAs produced from hot sheath protons, ENAs produced by the wings of the upstream solar wind distribution, ENAs scattered into the shadow by the limb atmosphere [*Brinkfeldt et al*., 2006; *Kallio et al*., 2006], or protons bent by ambient magnetic fields after reconverting to charged form.

MAVEN has sampled altitudes below the main absorption peak in two locations. As shown in Figure 1, for nominal periapsis altitudes near the terminator, we sample altitudes below the main absorption layer. In addition, during its second "deep dip" campaign, near the subsolar point, MAVEN also reached altitudes below the main absorption layer. In Figure 3, we can clearly identify both of these features as a reduction in penetrating proton density below the main peak. In these locations, the penetrating population not only decreases in density but also displays some energy loss, presumably resulting from the large number of collisions.

4. Relative Charge State Abundances of Penetrating Solar Wind Hydrogen

Some fraction of penetrating solar wind hydrogen ENAs should undergo electron attachment rather than electron stripping in the atmosphere, converting to H^- rather than H^+. High fluxes of ionospheric photoelectrons at periapsis make it difficult to observe this charge state, but at times we can measure a negatively charged hydrogen population with the Solar Wind Electron Analyzer (SWEA) instrument [*Mitchell et al*., 2015]. Figure 4 shows two orbits on 8 March 2015, preceding and subsequent to a high-speed interplanetary coronal mass ejection (CME). During each of these orbits, we measure both the upstream solar wind outside of the bow shock and a penetrating proton population with the same energy at periapsis. Before the CME, we can only pick out a very faint electron population at the same energy, with fluxes less than a factor of two above the ionospheric spectrum. However, after the CME, when the peak solar wind differential energy flux increases by a factor of ~3 and the energy more than doubles, increasing the height of the H^- peak and moving it to an energy range with lower ionospheric photoelectron flux, we can clearly identify the expected negative ion population with SWEA. The observed ratio of H^- to H^+ abundances, on the order of 1:10, suggests a similar ratio for the electron attachment and stripping cross sections (the relevant charge exchange back reactions will of course also play a role in the equilibrium fractionation). Laboratory data indeed indicate a ratio on the order of 1:10 between electron capture and electron loss cross sections for 1 keV hydrogen in CO_2 [*Lindsay et al*., 2005] and a ratio of 1:10 to 1:20 over a broader range of energy for N_2 and O_2 [*Van Zyl et al*., 1978], often used as proxies for CO_2 [*Kallio and Barabash*, 2001].

Thanks to a lack of natural ionospheric ions at these energies, ion measurements provide a higher-signal diagnostic of the penetrating ENA populations, but both ion and electron data provide a valuable probe of collisional processes occurring in the Martian atmosphere.

We note in conclusion that during this highly disturbed time, the flux of penetrating ENAs increases to such a high level that reconverted protons fill almost the entire magnetospheric volume sampled by MAVEN, extending to altitudes of thousands of kilometers in the downstream flank. Given the narrow energy signature seen throughout, this population most likely represents reconverted ENAs of solar wind origin scattered from the limb atmosphere rather than a product of diffuse ENAs produced in the sheath.

5. Implications and Conclusions

MAVEN ion and electron observations at low altitudes provide a new way of measuring penetrating solar wind hydrogen ENAs produced upstream from Mars. Given the low background and high signal of plasma spectrometers, this allows a highly sensitive measurement of the energy and angular distribution of both penetrating and backscattered ENAs, given reasonable assumptions about the conversion processes and the charged fraction that results. Numerous aspects remain to be studied, including the effects of crustal magnetic fields (not yet well sampled at low altitude by MAVEN), which may introduce significant changes in penetrating hydrogen deposition and backscatter, since magnetic deflection should have some effect even if penetrating hydrogen atoms spend only 5–10% of their transit time through the atmosphere in charged form. Intriguingly, results from MEX suggest a significant change in levels of backscattered ENAs in regions with strong crustal magnetic fields [*Wang et al*., 2013].

Already penetrating proton measurements enable remote monitoring of the solar wind velocity and with some model-based and/or empirical assumptions also provide a proxy measurement of the solar wind density. Furthermore, given a near-simultaneous measurement of the solar wind (either in a different orbit segment by MAVEN or from MEX), the ratio of the penetrating and backscattered proton fluxes to the upstream solar wind flux and their relative spectral forms can inform us about both the distant hydrogen corona and the charge exchange that takes place there, as well as the low-altitude atmosphere and the collisional processes therein.

At Earth, similar populations of precipitating hydrogen produce UV emission known as "proton aurora," identified by a characteristic Doppler shift from the velocity of the precipitating hydrogen [*Eather*, 1967]. One might find it interesting to speculate on whether one could observe a similar signature at Mars, and if so, what spatial organization and temporal dependence it would have.

Finally, while quiet time rates of solar wind hydrogen deposition in the atmosphere should not prove significant, during extreme events, solar wind deposition may provide a significant source term of hydrogen to the Martian system, albeit one that involves the removal of another planetary particle, since the initial charge exchange reaction will produce a pickup ion. For instance, given the very high solar wind flux on the order of $8\times10^8\,\mathrm{cm}^{-2}\,\mathrm{s}^{-1}$ during the 8 March 2015 CME of Figure 4, we can infer solar wind hydrogen deposition in the atmosphere on the order of $2\times10^7\,\mathrm{cm}^{-2}\,\mathrm{s}^{-1}$, comparable to the thermal escape flux of hydrogen for at least some time periods [*Chaffin et al.*, 2014]. Early in the solar system's history, solar wind flux and/or solar activity were likely stronger, potentially making solar wind accretion a more important source of hydrogen and perhaps even affecting the Deuterium/Hydrogen (D/H) ratio of the atmosphere.

Acknowledgments
We acknowledge the efforts of a terrific team of engineers and scientists over more than a decade to make the MAVEN mission and its state-of-the-art instrumentation a reality. Analysis of SWEA data was partially supported by CNES. MAVEN data are publicly available through the Planetary Data System.

The Editor thanks Herbert Gunell and Niklas Edberg for their assistance in evaluating this paper.

References

Anderson, D. E., Jr. (1974), Mariner 6, 7, and 9 ultraviolet spectrometer experiment: Analysis of hydrogen Lyman alpha data, *J. Geophys. Res.*, *79*, 1513–1518, doi:10.1029/JA079i010p01513.

Barabash, S., R. Lundin, R. Zarnowiecki, and S. Grzedzielski (1995), Diagnostic of energetic neutral particles at Mars by the ASPERA-C instrument for the Mars 96 mission, *Adv. Space Res.*, *16*, 81–86.

Brinkfeldt, K., et al. (2006), First ENA observations at Mars: Solar-wind ENAs on the nightside, *Icarus*, *182*, 439–447.

Connerney, J. E. P., J. Espley, P. Lawton, S. Murphy, J. Odom, R. Oliverson, and D. Sheppard (2015), The MAVEN magnetic field investigation, *Space Sci. Rev.*, doi:10.1007/s11214-015-0169-4.

Chaffin, M. S., J.-Y. Chaufray, I. Stewart, F. Montmessin, N. M. Schneider, and J.-L. Bertaux (2014), Unexpected variability of Martian hydrogen escape, *Geophys. Res. Lett.*, *41*, 314–320, doi:10.1002/2013GL058578.

Chaufray, J. Y., J. L. Bertaux, F. Leblanc, and E. Quémerais (2008), Observation of the hydrogen corona with SPICAM on Mars Express, *Icarus*, *195*, 598–613, doi:10.1016/j.icarus.2008.01.009.

Diéval, C., et al., (2012), A case study of proton precipitation at Mars: Mars Express observations and hybrid simulations, *J. Geophys. Res.*, *117*, A06222, doi:10.1029/2012JA017537.

Diéval, C., G. Stenberg, H. Nilsson, and S. Barabash (2013), A statistical study of proton precipitation onto the Martian upper atmosphere: Mars Express observations, *J. Geophys. Res. Space Physics*, *118*, 1972–1983, doi:10.1002/jgra.50229.

Eather, R. H. (1967), Auroral proton precipitation and hydrogen emissions, *Phys. Rev.*, *5*, 207–285.

Edberg, N., D. A. Brain, M. Lester, S. W. H. Cowley, R. Modolo, M. Fraenz, and S. Barabash (2009), Plasma boundary variability at Mars as observed by Mars Global Surveyor and Mars Express, *Ann. Geophys.*, *27*, 3537–3550.

Edberg, N. J. T., M. Lester, S. W. H. Crowley, D. A. Brain, M. Franz, and S. Barabash (2010), Magnetosonic Mach number effect of the position of the bow shock at Mars in comparison to Venus, *J. Geophys. Res.*, *115*, A07203, doi:10.1029/2009JA014998.

Futaana, Y., et al. (2006), First ENA observations at Mars: ENA emissions from the Martian upper atmosphere, *Icarus*, *182*, 424–430.

Gunell, H., et al. (2006), First ENA observations at Mars: Charge exchange ENAs produced in the magnetosheath, *Icarus*, *182*(2), 431–438, doi:10.1016/j.icarus.2005.10.027.

Halekas, J. S., E. R. Taylor, G. Dalton, G. Johnson, D. W. Curtis, J. P. McFadden, D. L. Mitchell, R. P. Lin, and B. M. Jakosky (2013), The Solar Wind Ion Analyzer for MAVEN, *Space Sci. Rev.*, doi:10.1007/s11214-013-0029-z.

Holmström, M., S. Barabash, and E. Kallio (2002), Energetic neutral atoms at Mars 1: Imaging of solar wind protons, *J. Geophys. Res.*, *107*(A10), 1277, doi:10.1029/2001JA000325.

Kallio, E., and S. Barabash (2001), Atmospheric effects of precipitating energetic hydrogen atoms on the Martian atmosphere, *J. Geophys. Res.*, *106*, 165–177, doi:10.1029/2000JA002003.

Kallio, E., J. G. Luhmann, and S. Barabash (1997), Charge exchange near Mars: The solar wind absorption and energetic neutral atom production, *J. Geophys. Res.*, *102*, 22,183–22,197, doi:10.1029/97JA01662.

Kallio, E., et al. (2006), Energetic Neutral Atoms (ENA) at Mars: Properties of the hydrogen atoms produced upstream of the Martian bow shock and implications for ENA sounding technique around non-magnetized planets, *Icarus*, *182*, 448–463.

Lindsay, B. G., W. S. Yu, and R. F. Stebbings (2005), Cross sections for charge-changing processes involving kilo-electron volt H and H^+ with CO and CO_2, *Phys. Rev. A*, *71*, 032705, doi:10.1103/PhysRevA.71.032705.

Mahaffy, P. R., et al. (2014), The neutral gas and ion mass spectrometer on the Mars atmosphere and volatile evolution mission, *Space Sci. Rev.*, doi:10.1007/s11214-014-0091-1.

McFadden, J., et al. (2015), The MAVEN suprathermal and thermal Ion composition (STATIC) instrument, *Space Sci. Rev.*

Mitchell, D. L., C. Mazelle, J. A. Sauvaud, D. Toublanc, R. Thocaven, A. Federov, E. R. Taylor, M. Robinson, P. Turin, and D. W. Curtis (2015), The MAVEN Solar Wind Electron Analyzer (SWEA), *Space Sci. Rev.*

Mura, A., et al. (2007), ENA detection on the dayside of Mars: ASPERA-3 NPD statistical study, *Planet. Space Sci.*, *56*, 840–845.

Van Zyl, B., H. Neumann, T. Q. Le, and R. C. Amme (1978), H + N_2 and H + O_2 collisions: Experimental charge-production cross sections and differential scattering calculations, *Phys. Rev. A*, *18*, 506–516.

Verigin, M. I.et al. (1999), Shape and location of planetary bow shocks, *Cosmic Res.*, *37*, 34.

Wang, X.-D., S. Barabash, Y. Futaana, A. Grigoriev, and P. Wurz (2013), Directionality and variability of energetic neutral hydrogen fluxes observed by Mars Express, *J. Geophys. Res. Space Physics*, *118*, 7635–7642, doi:10.1002/2013JA018876.

Wang, X.-D., S. Barabash, Y. Futaana, A. Grigoriev, and P. Wurz (2014), Influence of Martian crustal magnetic anomalies on the emission of energetic neutral hydrogen atoms, *J. Geophys. Res. Space Physics*, *119*, 8600–8609, doi:10.1002/2014JA020307.